Coupling Light into Graphene Plasmons through Surface Acoustic Waves

Jürgen Schiefele,[1,*] Jorge Pedrós,[2,3,†] Fernando Sols,[1,3] Fernando Calle,[2,3] and Francisco Guinea[4]

[1]*Departamento de Física de Materiales, Universidad Complutense de Madrid, E-28040 Madrid, Spain*
[2]*Instituto de Sistemas Optoelectrónicos y Microtecnología, Universidad Politécnica de Madrid, E-28040 Madrid, Spain*
[3]*Campus de Excelencia Internacional, Campus Moncloa UCM-UPM, E-28040 Madrid, Spain*
[4]*Instituto de Ciencia de Materiales de Madrid, CSIC, E-28049 Madrid, Spain*

(Received 3 September 2013; published 5 December 2013)

We propose a scheme for coupling laser light into graphene plasmons with the help of electrically generated surface acoustic waves. The surface acoustic wave forms a diffraction grating which allows us to excite the long lived phononlike branch of the hybridized graphene plasmon-phonon dispersion with infrared laser light. Our approach avoids patterning the graphene sheet, does not rely on complicated optical near-field techniques, and allows us to electrically switch the coupling between far-field radiation and propagating graphene plasmons.

DOI: 10.1103/PhysRevLett.111.237405 PACS numbers: 78.67.Wj, 73.20.Mf, 77.65.Dq

Surface plasmon polaritons (hereafter called plasmons) are electromagnetic waves that are confined to the interface between two materials and accompanied by collective oscillations of surface charges [1]. The strong spatial confinement of the electromagnetic field and its coupling to charge carriers allow for the manipulation of light at subwavelength scales—beyond the diffraction limit of classical optics—which opens the possibility to integrate electronics and optics at the nanoscale. Further promising plasmonic applications include single molecule detection, metamaterials, and light harvesting [2].

Graphene, a single layer of carbon atoms arranged in a honeycomb lattice [3], forms a pure two-dimensional electron gas that supports plasmons in a broad frequency range from the midinfrared to the terahertz domain [4–6]. Unlike conventional plasmons in noble metals, graphene plasmons can be tuned *in situ* through the modulation of the carrier density by electrostatic gating. For long wavelengths $k \ll k_F$, the plasmon wave vector in graphene on a (nonpolar) dielectric substrate is approximately given by [7]

$$k = \frac{\omega_p}{c}\frac{E_p}{E_F}\frac{\epsilon_{\mathrm{eff}}}{2\alpha_{\mathrm{fs}}}, \tag{1}$$

where $E_p = \hbar\omega_p$ is the plasmon energy, $\epsilon_{\mathrm{eff}} = (\epsilon_\infty + 1)/2$ the effective average over the dielectric constants of substrate and air, and the Fermi energy $E_F = \hbar v_F\sqrt{\pi n}$ can be adjusted with the carrier density n. The strong field concentration typical for plasmon excitations results in a large wave vector mismatch $k \gg \omega_p/c$, which is revealed by the small magnitude of the fine-structure constant $\alpha_{\mathrm{fs}} \simeq 1/137$ in Eq. (1). Therefore, the excitation of plasmons with free-space radiation requires diffraction of the incident light at structures with dimensions smaller than $2\pi c/\omega_p$. In the experiments realized so far, graphene-plasmon laser coupling required either complex near-field techniques [8,9] or the patterning of micro- or nanoscale arrays for far-field coupling [10–13], where edge scattering reduces the plasmon lifetime. In this work, we propose a scheme for converting far-field radiation into graphene plasmons by deforming the graphene sheet with a surface acoustic wave (SAW) and thus forming a tunable optical grating without the need of any patterning. Our calculation shows that long-lived midinfrared plasmons, hybridized with surface phonons in the supporting piezoelectric materials, are excited with good efficiencies. Figure 1 shows a sketch of the proposed device, where a high-frequency signal applied to an interdigital transducer (IDT) on a piezoelectric film generates a Rayleigh-type SAW propagating in the x direction. The graphene sheet is periodically deformed in the x-z plane by the strain field of the wave. Thus, a propagating grating with an adjustable amplitude up to a few nanometers and a period in the submicron range can be formed. By diffraction on the grating, incident TM polarized laser light (that is, with its **E** field polarized in the x-z-plane) can overcome the momentum mismatch and excite plasmons in the graphene sheet. AlN and ZnO have been selected as piezoelectric materials since they present large electromechanical coupling coefficients and

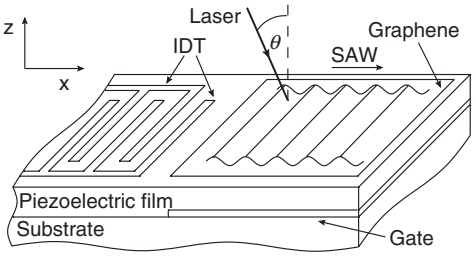

FIG. 1. Sketch of the device. A high-frequency signal applied to an interdigital transducer (IDT) on a piezoelectric film generates a surface acoustic wave (SAW) propagating in the x direction. The graphene sheet is deformed by the SAW, the periodic deformation acting as a refraction grid for the incident laser beam. A back gate allows tuning the Fermi energy of graphene.

their high-quality thin films can be deposited by sputtering on a variety of substrates [14,15]. Submicron IDTs on these materials allow SAWs operating well above 10 GHz [15,16]. A back gate, deposited on the substrate before sputtering the film, allows us to tune the graphene plasmon dispersion in and out of resonance with the laser.

The material underneath the graphene influences its electronic properties, as the charge carriers in graphene couple to the long-range electric fields generated by optically active phonon modes in the surrounding material [17]. This mechanism is known to influence charge transport and drag effects in graphene [18–20], as well as to alter the dispersion of graphene plasmons on polar substrates [12,21].

Piezoelectric materials are polar by definition. For the dielectric function of the piezoelectric film, an oscillator model is assumed:

$$\epsilon(\omega) = \epsilon_\infty + (\epsilon_0 - \epsilon_\infty)\frac{\omega_{\mathrm{TO}}^2}{\omega_{\mathrm{TO}}^2 - \omega^2 + 2i\omega\Gamma}, \quad (2)$$

where ω_{TO} denotes the frequency of the transverse optical phonon, Γ its damping rate, and ϵ_0 and ϵ_∞ the static and high-frequency dielectric constants, respectively. The coupling strength between carriers in the graphene sheet and polar surface phonons (with frequency ω_{sp}) located at the surface of the piezoelectric film is given by [17,19,22]

$$M(\mathbf{k}) = g e^{-kz_0}\sqrt{\pi c \alpha_{\mathrm{fs}} \hbar^2 \omega_{\mathrm{sp}}/k}. \quad (3)$$

Here, $\mathbf{k} = (k_x, k_y)$ is the surface-phonon wave vector, the coupling constant $g = \{(\epsilon_0 - \epsilon_\infty)/[(1 + \epsilon_\infty)(1 + \epsilon_0)]\}^{1/2}$, $z_0 > 0$ denotes the graphene-substrate separation, and ω_{sp} is the solution of the equation $1 + \epsilon(\omega) = 0$. As the wave vector range of interest here is $k \approx 10^7\ \mathrm{m}^{-1}$ and $z_0 \approx 3$ Å for the common substrate materials, the exponential factor has been set to unity in the following. Apart from the coupling to substrate phonons, graphene electrons also couple to in-plane optical and out-of-plane (flexural) phonon modes in the graphene sheet itself. While the former would play a role only at plasmon energies above 200 meV [12], which are out of our parameter range, the latter process is strongly suppressed in substrate supported graphene sheets [23,24], and in the following, we neglect both of these scattering mechanisms.

Because of the coupling $M(k)$, charge carriers in the graphene sheet can interact by exchange of surface phonons, which leads to the potential [21]

$$V_{\omega_{\mathrm{sp}}}(k, \omega, \tau_{\mathrm{sp}}) = |M(k)|^2 G_{\omega_{\mathrm{sp}}}(\omega, \tau_{\mathrm{sp}}), \quad (4)$$

where the lifetime of the surface phonon τ_{sp} enters the phonon propagator

$$G_{\omega_{\mathrm{sp}}}(\omega, \tau_{\mathrm{sp}}) = \frac{2\omega_{\mathrm{sp}}}{\hbar[(\omega + i/\tau_{\mathrm{sp}})^2 - \omega_{\mathrm{sp}}^2]}. \quad (5)$$

For AlN ($\epsilon_0 = 7.37$, $\epsilon_\infty = 3.93$) we obtain $g = 0.289$ and $\hbar\omega_{\mathrm{sp}} = 106$ meV, for ZnO ($\epsilon_0 = 7.46$, $\epsilon_\infty = 3.61$), $g = 0.314$ and $\hbar\omega_{\mathrm{sp}} = 68$ meV [25].

The total effective carrier interaction results from Coulomb interaction $V_C = e^2/(2k\epsilon_{\mathrm{vac}}\epsilon_{\mathrm{eff}})$ [with $\epsilon_{\mathrm{vac}} = e^2/(4\pi\hbar\alpha_{\mathrm{fs}}c)$ the permittivity of free space] and phonon exchange. Within the random phase approximation (RPA), it reads [21,28]

$$V_{\mathrm{RPA}}^{\mathrm{eff}} = \frac{V_C + V_{\omega_{\mathrm{sp}}}}{1 - (V_C + V_{\omega_{\mathrm{sp}}})\Pi^{(0)}} = \frac{V_C}{\epsilon_{\mathrm{RPA}}}, \quad (6)$$

where $\Pi^{(0)}$ denotes the polarizability of graphene [29,30] which depends parametrically on the electron relaxation time τ_e [31]. The last equality in Eq. (6) defines the total dielectric screening function $\epsilon_{\mathrm{RPA}}(k, \omega)$. The plasmon dispersion can be obtained by (numerically) solving the equation $\epsilon_{\mathrm{RPA}}(k, \omega) = 0$, which depends on the dielectric function of the piezoelectric film via $V_{\omega_{\mathrm{sp}}}$ in Eq. (6). An approximate analytical expression can be obtained from Eq. (6) by setting the scattering times τ_{sp}, $\tau_e \to \infty$ and $\Pi^{(0)} \approx E_F k^2/(\pi\hbar^2\omega^2)$, which is valid for $\omega > v_F k$ and $E_F \gg \hbar\omega$. Solving for the zeros of ϵ_{RPA} yields the two solutions

$$\omega_{p\pm}^2(k) = \frac{1}{2}[\omega_{\mathrm{sp}}^2 + \omega_p^2 \pm \sqrt{(\omega_{\mathrm{sp}}^2 + \omega_p^2)^2 - 4\omega_p^2\omega_{\mathrm{sp}}^2(1 - 2g^2\epsilon_{\mathrm{eff}})}], \quad (7)$$

where $\omega_p(k)$ is given by Eq. (1). The two branches $\omega_{p\pm}$ shown as white curves in Figs. 2(a) and 2(c) describe coupled excitations involving both collective electronic and lattice oscillations. In the limit $g \to 0$ of vanishing substrate coupling, $\omega_{p+} \to \omega_{\mathrm{sp}}$ and $\omega_{p-} \to \omega_p$, and the unhybridized system is recovered.

The plasmon lifetimes τ_p shown in Figs. 2(b) and 2(d)—of the order of 10^{-13} s—are obtained by solving the equation $\epsilon_{\mathrm{RPA}} = 0$ for the imaginary part of the plasmon frequency. As a function of frequency, they vary between the boundaries set by the surface-phonon damping τ_{sp}, assumed to be 1 ps as reported in Ref. [12], and the electron relaxation time of graphene, $\tau_e = \mu E_F/v_F^2$, where μ is the carrier mobility. For low k values, the ω_{p+} branch is dominated by τ_{sp} rather than τ_e, allowing us to excite relatively long-lived plasmons. In the limit $k \to 0$, $\tau_p = \tau_{\mathrm{sp}}$. Conversely, the ω_{p-} branch shows a stronger damping, due to the larger influence of τ_e.

Plasmon excitation manifests itself in enhanced light absorption. The transmittance and reflectance of graphene on a dielectric substrate can be calculated from the Fresnel reflection and transmission coefficients [32]

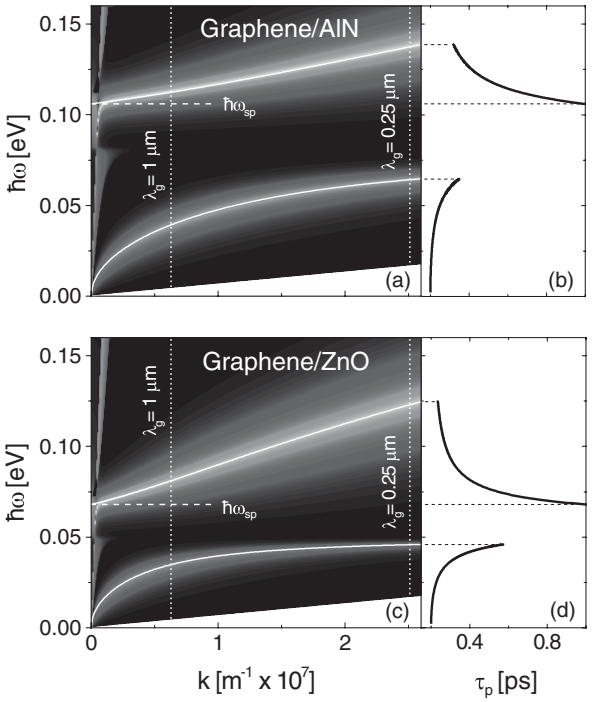

FIG. 2. (a), (c) Plasmon dispersion for graphene on AlN and on ZnO, respectively. The two hybridized plasmon branches are well described by the asymptotic expressions $\omega_{p\pm}(k)$ of Eq. (7) (white curves). The contour plot shows the imaginary part of the reflection coefficient $r^{\mathrm{TM}}(k, \omega)$; see Eq. (8a). Parameters are $E_F = 0.4$ eV and $\tau_e = 2 \times 10^{-13}$ s (corresponding to a mobility of 5000 $\mathrm{cm^2\,V^{-1}\,s^{-1}}$). The white triangular area indicates the region of high intraband loss, $\omega < v_F k$. (b), (d) Plasmon lifetime τ_p along the two branches.

$$r^{\mathrm{TM}}(k, \omega) = \frac{\epsilon(\omega)k_z - k_z' + \sigma(\omega)k_z k_z'/(\epsilon_{\mathrm{vac}}\omega)}{\epsilon(\omega)k_z + k_z' + \sigma(\omega)k_z k_z'/(\epsilon_{\mathrm{vac}}\omega)}, \tag{8a}$$

$$t^{\mathrm{TM}}(k, \omega) = \frac{2\sqrt{\epsilon(\omega)}k_z}{\epsilon(\omega)k_z + k_z' + \sigma(\omega)k_z k_z'/(\epsilon_{\mathrm{vac}}\omega)}, \tag{8b}$$

$$r^{\mathrm{TE}}(k, \omega) = t^{\mathrm{TE}} - 1 = \frac{k_z - k_z' - \omega\sigma(\omega)/(c^2\epsilon_{\mathrm{vac}})}{k_z + k_z' + \omega\sigma(\omega)/(c^2\epsilon_{\mathrm{vac}})}, \tag{8c}$$

where TM and TE denote the polarization of the incident beam, $k_z = \sqrt{(\omega/c)^2 - k^2}$ and $k_z' = \sqrt{\epsilon(\omega)(\omega/c)^2 - k^2}$ are the z components of the wave vector in air and in the substrate, respectively, and

$$\sigma(\omega) = \frac{e^2 E_F}{\pi\hbar^2}\frac{i}{\omega + i/\tau_e} + \frac{e^2}{4\hbar}\left[\Theta(\hbar\omega - 2E_F) + \frac{i}{\pi}\log\left|\frac{\hbar\omega - 2E_F}{\hbar\omega + 2E_F}\right|\right] \tag{9}$$

is the conductivity of graphene at zero temperature [31], which yields a good approximation as long as $T \ll T_F$. In the nonretarded limit $\omega/c \ll k$, the zeros of ϵ_{RPA} are identical to the poles of r^{TM}. Correspondingly, the absorption of light given by $\mathrm{Im}r^{\mathrm{TM}}$ [shown by the contour plots in Figs. 2(a) and 2(c)] displays peak values along the two branches $\omega_{p\pm}$ of Eq. (7).

Figure 3(a) shows the transmittance through the air-graphene-AlN (red curve) and air-AlN (blue curve) interface in the frequency range $\hbar\omega = 0$-0.2 eV for normal incident light. A region of low transmittance is observed between the transverse and longitudinal optical phonon frequencies of AlN. In the presence of graphene, the transmittance at low frequencies is reduced due to the Drude response. Within the frequency range of the ω_{p+} branch, both AlN and graphene-AlN are seen to be almost transparent.

In the presence of the SAW, the transmittance changes, because a TM polarized laser beam can overcome the momentum mismatch and excite plasmons: the SAW imposes a sinusoidal deformation of wavelength λ_g and amplitude δ on the graphene. This corrugation works like a diffraction grating that scatters incident light with wave vector $(k_{\parallel 0}, k_{z0})$ into the various diffraction orders $(k_{\parallel m}, k_{zm})$, with

$$k_{\parallel m} = (\omega/c)\sin\theta + m2\pi/\lambda_g, \tag{10}$$

$$k_{zm} = \sqrt{(\omega/c)^2 - k_{\parallel m}^2}, \tag{11}$$

where θ denotes the angle of off-normal incidence and m is an integer. To excite plasmons, the frequency of the plasmon has to coincide with the laser frequency, and its k vector with one of the $k_{\parallel m}$, which in turn can be chosen by an appropriate SAW wavelength λ_g [33].

The intensity of the diffracted light in mth order, normalized to the intensity of the incoming beam, is given by [34]

$$I^{(m)} = \left| rJ_m(2k_{z0}\delta)\left[1 + \frac{m\pi}{\lambda_g k_{zm}}\frac{1+r}{r}\right]\right|^2. \tag{12}$$

Here, r denotes, depending on the polarization of incident light, $r^{\mathrm{TM}}(\omega, k_{\parallel m})$ or $r^{\mathrm{TE}}(\omega, k_{\parallel m})$ [see Eqs. (8)]. As the corrugation amplitude δ achievable with SAWs is of the order of a few nanometers, $k_{z0}\delta \ll 1$, and the relative intensities $I^{(m)}$ are suppressed proportionally to the Bessel function $|J_m(2k_{z0}\delta)|^2 \simeq (k_{z0}\delta)^{2m}$.

The range of wave vectors in which plasmons can be excited is determined by λ_g, i.e., by the period of the IDT. With electron-beam or nanoimprint lithography, periods of 0.25–1 μm can be realized [14–16]. For normal incidence, $k_{\parallel 1}$ then takes values between $(0.6\text{–}2.5) \times 10^7\ \mathrm{m^{-1}}$, as indicated by the vertical dotted lines in Figs. 2(a) and 2(c). For $k_{\parallel 1}$ within this range and ω along the plasmon dispersion, k_{z1} is imaginary, and the electric field of the diffracted beam decays exponentially in the direction perpendicular to the surface.

The transmittance T in the presence of a SAW (with $\lambda_g = 0.25$ μm and $E_F = 0.4$ eV) is shown in Fig. 3(b) for TE and TM polarization (red and black curves, respectively). While the former does not deviate from the

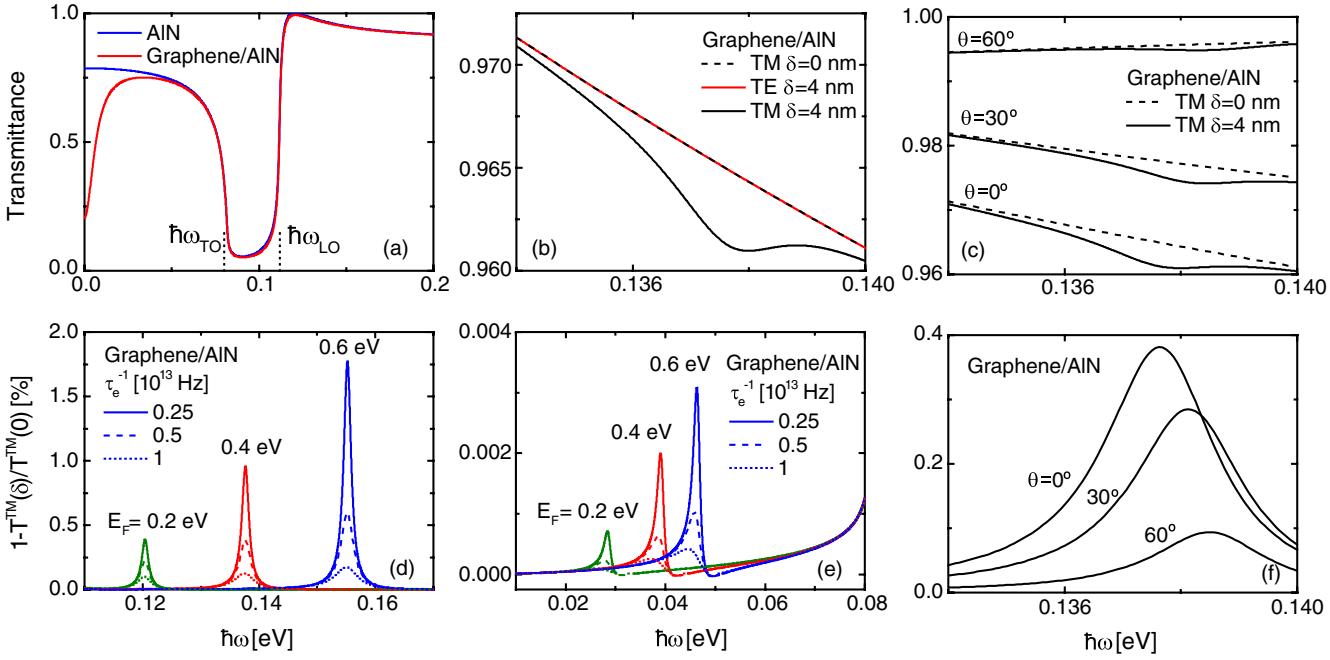

FIG. 3 (color online). (a) Transmittance of AlN and graphene on AlN in the absence of surface corrugation, normal incident light. (b) Change in the transmittance of TM polarized light due to plasmon excitation in the presence of a SAW. SAW amplitude $\delta = 4$ nm and period $\lambda_g = 0.25$ μm, graphene parameters E_F and τ_e as in Fig. 2. (c) Same as (b) for various angles of incidence θ. (d) Extinction spectrum of graphene on AlN in the presence of a SAW ($\delta = 4$ nm and $\lambda_g = 0.25$ μm) for different values of E_F and τ_e. Peaks are due to excitation of plasmons in the ω_{p+} branch [see Eq. (7)]. (e) Same as (d) for excitation of plasmons in the ω_{p-} branch, $\delta = 4$ nm and $\lambda_g = 1$ μm. (f) Extinction spectrum corresponding to (c).

transmittance at an uncorrugated interface (black dashed curve), the latter displays a dip due to plasmon excitation in the ω_{p+} branch. As the two plasmon branches get steeper with increasing E_F, the plasmon resonance blueshifts. This is shown in the extinction spectra $1 - T^{\mathrm{TM}}(\delta)/T^{\mathrm{TM}}(0)$ of Figs. 3(d) and 3(e) for the $\omega_{p\pm}$ branches, respectively. The height of the peaks can serve as a figure of merit for the efficiency of plasmon excitation. For fixed E_F and λ_g, it depends on the graphene quality through the electron relaxation time τ_e. The solid, dashed, and dotted curves in Figs. 3(d) and 3(e) were obtained by setting τ_e^{-1} to 0.25, 0.5, and 1×10^{13} Hz, respectively. The height of the resonance increases with τ_e, as damping of the collective electron oscillations decreases. For $\hbar\omega \gtrsim 0.6$ eV, the plasmon resonance of the ω_{p-} branch in Fig. 3(e) begins to merge with the phonon resonances of AlN [see Fig. 3(a)]. As the intensity of incident light diffracted to second order [$m = 2$ in Eq. (12)] is smaller by a factor of 10^5 compared to the first order, extinction peaks due to the excitation of plasmons with wave vector $k_{\|2}$ are not visible on the scale of Figs. 3(d) and 3(e). The extinction spectra for graphene on ZnO are qualitatively similar to those shown for AlN, but allow us, due to the lower surface-phonon frequency, to excite ω_{p+} plasmons with longer laser wavelengths (see Fig. 2(c)].

As $\omega/c \ll 2\pi/\lambda_g$, the θ-dependent term in Eq. (10) shifts the plasmon resonance only slightly, as shown by the transmittance and extinction spectra in Figs. 3(c) and 3(f). The strength of the resonance, however, is maximal for normal incident light, because only the x component of the electric field excites plasmons.

Because of the δ^2 dependence in the diffraction intensity of Eq. (12), the achievable efficiency also depends strongly on the SAW amplitude. With the realistic value of 4 nm used in Fig. 3 [35], the predicted extinction values are comparable to those obtained in Ref. [12] with patterned graphene. However, exciting plasmons in an extended graphene sheet avoids plasmon damping due to edge scattering, which severely limits plasmon lifetimes in patterned graphene [12]. Moreover, the SAW-assisted plasmon generation mechanism in homogeneous graphene will permit us to design plasmonic devices using propagating plasmons, otherwise impeded in patterned graphene structures.

We have demonstrated that SAWs can be used to generate a switchable refraction grid which couples laser light into the hybridized plasmon supported by graphene on piezoelectric materials like, for example, ZnO and AlN. The coupling to surface phonons shifts the low wave vector part of the graphene plasmon dispersion, which is virtually unaffected by intraband losses, upwards into the attractive midinfrared frequency range. Because of their relatively low damping in the vicinity of the surface-phonon frequency, these phononlike plasmon branches have a high potential for photonic applications.

The proposed scheme for plasmon excitation avoids the patterning of graphene, diminishing the edge scattering and generating propagating plasmons which could be used in future graphene-based plasmonic devices. Moreover, plasmons can be switched electrically, via the high-frequency signal at the IDT, whereas the plasmon resonance can be tuned via electrostatic gating. In addition, the IDT technology allows for many different plasmon functionalities. For example, curved IDTs can create interfering SAWs for plasmon focusing [36]. Thus, SAWs offer the possibility to tailor electrically switchable graphene-based metamaterials.

We would like to thank Frank Koppens, Christopher Gaul, and Harald Haakh for helpful remarks. The authors acknowledge support from the Marie Curie ITN *NanoCTM*, the Campus de Excelencia Internacional (Campus Moncloa UCM-UPM), ERC Advanced Grant No. 290846, and MICINN (Spain) through Grants No. FIS2008-00124, No. FIS2010-21372, No. TEC2010-19511, and No. FIS2011-23713.

Note added in proof.—After this Letter was accepted for publication, we became aware of related work reporting a different technique to excite graphene plasmons through excitation of elastic vibrations [37].

*jurgesch@ucm.es
†j.pedros@upm.es

[1] S. A. Maier, *Plasmonics: Fundamentals and Applications* (Springer, New York, 2007).
[2] A. Polman, Science **322**, 868 (2008).
[3] A. H. C. Neto, F. Guinea, N. M. R. Peres, K. S. Novoselov, and A. K. Geim, Rev. Mod. Phys. **81**, 109 (2009).
[4] F. H. L. Koppens, D. E. Chang, and F. J. Garcia de Abajo, Nano Lett. **11**, 3370 (2011).
[5] A. N. Grigorenko, M. Polini, and K. S. Novoselov, Nat. Photonics **6**, 749 (2012).
[6] Y. V. Bludov, A. Ferreira, N. M. R. Peres, and M. I. Vasilevskiy, Int. J. Mod. Phys. B **27**, 1341001 (2013).
[7] This relation follows from a semiclassical (Drude) model for the graphene conductivity, which only takes into account the first term of Eq. (9) and neglects disorder, $\tau_e \rightarrow \infty$.
[8] J. Chen, M. Badioli, P. Alonso-Gonzalez, S. Thongrattanasiri, F. Huth, J. Osmond, M. Spasenovic, A. Centeno, A. Pesquera, P. Godignon *et al.*, Nature (London) **487**, 77 (2012).
[9] Z. Fei, A. S. Rodin, G. O. Andreev, W. Bao, A. S. McLeod, M. Wagner, L. M. Zhang, Z. Zhao, M. Thiemens, G. Dominguez *et al.*, Nature (London) **487**, 82 (2012).
[10] L. Ju, B. Geng, J. Horng, C. Girit, M. Martin, Z. Hao, H. A. Bechtel, X. Liang, A. Zettl, Y. R. Shen *et al.*, Nat. Nanotechnol. **6**, 630 (2011).
[11] A. Y. Nikitin, F. Guinea, F. J. García-Vidal, and L. Martín-Moreno, Phys. Rev. B **84**, 161407 (2011).
[12] H. Yan, T. Low, W. Zhu, Y. Wu, M. Freitag, X. Li, F. Guinea, P. Avouris, and F. Xia, Nat. Photonics **7**, 394 (2013).
[13] M. Freitag, T. Low, W. Zhu, H. Yan, F. Xia, and P. Avouris, Nat. Commun. **4**, 1951 (2013).
[14] J. Pedrós, L. García-Gancedo, C. J. B. Ford, J. P. Griffiths, G. A. C. Jones, and A. J. Flewitt, Appl. Phys. Lett. **102**, 043507 (2013).
[15] J. Rodríguez-Madrid, G. Iriarte, J. Pedrós, O. Williams, D. Brink, and F. Calle, IEEE Electron Device Lett. **33**, 495 (2012).
[16] S. Büyükköse, B. Vratzov, D. Ataç, J. van der Veen, P. V. Santos, and W. G. van der Wiel, Nanotechnology **23**, 315303 (2012).
[17] N. Mori and T. Ando, Phys. Rev. B **40**, 6175 (1989).
[18] J. Schiefele, F. Sols, and F. Guinea, Phys. Rev. B **85**, 195420 (2012).
[19] E. H. Hwang and S. Das Sarma, Phys. Rev. B **87**, 115432 (2013).
[20] B. Amorim, J. Schiefele, F. Sols, and F. Guinea, Phys. Rev. B **86**, 125448 (2012).
[21] E. H. Hwang, R. Sensarma, and S. D. Sarma, Phys. Rev. B **82**, 195406 (2010).
[22] S. Fratini and F. Guinea, Phys. Rev. B **77**, 195415 (2008).
[23] E. V. Castro, H. Ochoa, M. I. Katsnelson, R. V. Gorbachev, D. C. Elias, K. S. Novoselov, A. K. Geim, and F. Guinea, Phys. Rev. Lett. **105**, 266601 (2010).
[24] B. Amorim and F. Guinea, Phys. Rev. B **88**, 115418 (2013).
[25] Material parameters for AlN and ZnO are taken from Refs. [26,27], respectively.
[26] M. Kazan, S. Pereira, M. R. Correia, and P. Masri, J. Appl. Phys. **106**, 023523 (2009).
[27] N. Ashkenov, B. N. Mbenkum, C. Bundesmann, V. Riede, M. Lorenz, D. Spemann, E. M. Kaidashev, A. Kasic, M. Schubert, M. Grundmann *et al.*, J. Appl. Phys. **93**, 126 (2003).
[28] G. D. Mahan, *Many-Particle Physics* (Plenum, New York, 1981).
[29] B. Wunsch, T. Stauber, F. Sols, and F. Guinea, New J. Phys. **8**, 318 (2006).
[30] E. H. Hwang and S. Das Sarma, Phys. Rev. B **75**, 205418 (2007).
[31] M. Jablan, H. Buljan, and M. Soljačić, Phys. Rev. B **80**, 245435 (2009).
[32] R. Messina and P. Ben-Abdallah, Sci. Rep. **3**, 1383 (2013).
[33] C. Ruppert, J. Neumann, J. B. Kinzel, H. J. Krenner, A. Wixforth, and M. Betz, Phys. Rev. B **82**, 081416 (2010).
[34] E. C. Lean, in *Progress in Optics*, edited by E. Wolf (North-Holland, Amsterdam, 1973), Vol. XI, p. 123.
[35] R. Shilton, M. K. Tan, L. Y. Yeo, and J. R. Friend, J. Appl. Phys. **104**, 014910 (2008).
[36] L. Yin, V. K. Vlasko-Vlasov, J. Pearson, J. M. Hiller, J. Hua, U. Welp, D. E. Brown, and C. W. Kimball, Nano Lett. **5**, 1399 (2005).
[37] M. Farhat, S. Guenneau, and H. Bağcı, preceding Letter, Phys. Rev. Lett. **111**, 237404 (2013).